International Journal of Nanomedicine

Dovepress
open access to scientific and medical research

Open Access Full Text Article

ORIGINAL RESEARCH

Follicular delivery of spironolactone via nanostructured lipid carriers for management of alopecia

This article was published in the following Dove Press journal:
International Journal of Nanomedicine
26 November 2014
Number of times this article has been viewed

Rehab Nabil Shamma
Mona Hassan Aburahma

Department of Pharmaceutics and Industrial Pharmacy, Faculty of Pharmacy, Cairo University, Cairo, Egypt

Abstract: Spironolactone (SL) is a US Food and Drug Administration-approved drug for the treatment of hypertension and various edematous conditions. SL has gained a lot of attention for treating androgenic alopecia due to its potent antiandrogenic properties. Recently, there has been growing interest for follicular targeting of drug molecules for treatment of hair and scalp disorders using nanocolloidal lipid-based delivery systems to minimize unnecessary systemic side effects associated with oral drug administration. Accordingly, the objective of this study is to improve SL efficiency and safety in treating alopecia through the preparation of colloidal nanostructured lipid carriers (NLCs) for follicular drug delivery. SL-loaded NLCs were prepared by an emulsion solvent diffusion and evaporation method using 2^3 full factorial design. All of the prepared formulations were spherical in shape with nanometric size range (215.6–834.3 nm) and entrapment efficiency >74%. Differential scanning calorimetry thermograms and X-ray diffractograms revealed that SL exists in amorphous form within the NLC matrices. The drug release behavior from the NLCs displayed an initial burst release phase followed by sustained release of SL. Confocal laser scanning microscopy confirmed the potential of delivering the fluorolabeled NLCs within the follicles, suggesting the possibility of using SL-loaded NLCs for localized delivery of SL into the scalp hair follicles.

Keywords: spironolactone, androgenic alopecia, nanostructured lipid carriers, follicular targeting, confocal laser scanning microscopy

Introduction

Androgenic alopecia (AA) is a commonly encountered skin disorder in scalp hair follicles that causes pattern hair loss due to the elevation in the androgen level that fosters miniaturization of hair in the anagen stage, leading to balding.[1,2] In AA, most patients exhibit normal circulating androgen levels, yet they suffer from "cutaneous hyperandrogenism" resulting from in situ overexpression of the androgenic enzymes and hyper-responsiveness of androgen receptors within the skin's pilosebaceous unit.[2] A lot of difficulties face successful treatment interventions for AA, as only two medications (minoxidil and finasteride) are currently approved. However, these medications offer variable results, lack of a permanent cure, and potential complications.[3]

Spironolactone (SL) is a relatively old US Food and Drug Administration-approved therapeutic agent that is utilized primarily as a diuretic for managing different edematous conditions.[1] SL has potent antiandrogenic properties resulting from dual mechanisms: reduction of androgen production and competitive blockage of androgen receptors in target tissues.[1] SL's success in reducing AA after oral administration was confirmed in numerous case reports and trials.[3–6] This encouraged dermatologists to prescribe

Correspondence: Mona Hassan Aburahma
Department of Pharmaceutics and Industrial Pharmacy, Faculty of Pharmacy, Cairo University, Kasr El-Aini Street, 11562, Cairo, Egypt
Email mona_aburahma@hotmail.com

oral SL (200 mg daily). Nevertheless, this regimen is usually associated with dose-dependent adverse effects.[1,7]

Nanostructured lipid carriers (NLCs) represent a relatively new type of colloidal drug delivery system that consists of solid lipid and liquid lipid, and offers the advantage of improved drug loading capacity and release properties compared with solid lipid nanoparticles.[8] Currently, there is an increasing interest in follicular delivery of drugs using nanocolloidal lipid-based delivery systems for treatment of various disorders (acne, alopecia, and other sebaceous gland dysfunction) associated with the pilosebaceous structure.[9] Follicular targeting of drugs offers the advantages of reducing the drug dose along with decreasing systemic toxicity associated with oral drug administration.[9] Since AA is specifically restricted to pilosebaceous units, improving the outcome of alopecia therapy might be possible by increasing drug distribution in the target site within the hair follicles.

To our best knowledge, SL targeting into hair follicles via colloidal NLCs for treatment of AA through decreasing androgen production within sebaceous glands and blocking the androgen receptors in dermal papillae has not yet been investigated. Accordingly, the aim of the present work was to investigate the ability of follicular targeting of SL by encapsulation into colloidal NLCs to improve its therapeutic efficiency and avoid unnecessary side effects after oral administration.

Materials and methods

Materials

SL was kindly supplied by Eipico (Cairo, Egypt). Tween 80 and rhodamine B isothiocyanate were purchased from Sigma-Aldrich Chemical Co. (St Louis, MO, USA). Transcutol®P (diethylene glycol monoethyl ether) and Compritol®888 ATO (glycerylbehenate) were provided by Gattefosse (Saint-Priest, France). Spectrapore® nitrocellulose membranes (2,000–15,000 Mw cutoff) were obtained from Spectrapore Inc. (New York, NY, USA). Absolute ethanol, olive oil, and acetone were purchased from El-Nasr Chemical Co. (Cairo, Egypt). All other solvents were of analytical grade and were used as received.

Preparation of spironolactone-loaded nanostructured lipid carriers

Spironolactone-loaded nanostructured lipid carriers (SL-NLCs) were prepared by an emulsion solvent diffusion and evaporation method followed by ultrasonication, as reported by Eskandari et al[10] but with slight modification. Fifty milligrams of SL was dispersed in the liquid lipid (olive oil alone or containing 50% Transcutol®) then added to molten Compritol® at 5% or 15% levels with respect to total solid lipid in the formulation. Following that, 10 mL of acetone and ethanol mixture (1:1) was added to the lipids maintained in a water bath at 80°C until complete dissolution of lipids in the organic phase. The latter was dispersed in an aqueous solution containing Tween 80 (1% or 2%) at 80°C and mixed using a magnetic stirrer rotating at 1,000 rpm for 1 minute. The resulting pre-emulsion was then ultrasonicated for 3 minutes to produce an oil/water nanoemulsion that was cooled down at room temperature while stirring at 500 rpm until evaporation of the organic solvent to form SL-NLC dispersion.

Characterization of SL-NLCs

Determination of NLCs entrapment efficiency percentage

The entrapment efficiency (EE) of the SL-NLC formulation was estimated indirectly by determining the free SL in the dispersion medium according to the following equation:[11]

$$EE\ (\%) = \frac{\text{Total amount of SL} - \text{Amount of free SL}}{\text{Total amount of SL}} \times 100. \quad (1)$$

Determination of particle size, polydispersity index, and zeta potential

The average particle size (PS), polydispersity index (PI), and zeta potential (ZP) of the prepared NLCs were determined by Zetasizer Nano ZS (Malvern Instruments, Malvern, UK) after proper dilution of the samples with distilled water.

Study of the influence of different formulation parameters using 2^3 full factorial design

A complete 2^3 factorial design was used to optimize and evaluate the effect of different variables on the characteristics of SL-NLCs (Table 1). The independent variables were the percentage of liquid lipid with respect to total lipid mixture (X_1), percentage of surfactant in aqueous phase (X_2), and percentage of Transcutol® in liquid lipid (X_3). The EE% (Y_1), PS (Y_2), PDI (Y_3), and ZP (Y_4) were designated as the dependent variables.

The studied experimental responses were the results of the individual influences and the interactions of the three independent variables. A two-level experimental design provides sufficient data to fit the following polynomial equation:

$$Y = b_0 + b_1X_1 + b_2X_2 + b_3X_3 + b_{12}X_1X_2 + b_{13}X_1X_3 + b_{23}X_2X_3 \quad (2)$$

Table 1 Full factorial design used to optimize the spironolactone-loaded nanostructured lipid carrier formulations

	Level	
	Low (−1)	**High (1)**
Factors (independent variables)		
X_1: Percentage liquid lipid with respect to total lipid mixture	5	15
X_2: Percentage surfactant concentration in aqueous phase	1	2
X_3: Percentage of Transcutol® in liquid lipid	0	50
Response (dependent variables)	Constraints	
Y_1: EE%	Maximize	
Y_2: PS	Minimize	
Y_3: PI	Minimize	
Y_4: ZP	Maximize	

Abbreviations: EE, entrapment efficiency; PS, particle size; PI, polydispersity index; ZP, zeta potential.

where Y is the dependent variable, b_0 is the intercept term, and b_1–b_{23} are the coefficients for the factors X_1, X_2, and X_3 and their interaction terms.[12] The experimental results were analyzed by Design Expert® software version 7 (Stat-Ease, Inc., Minneapolis, MN, USA) to extract the main effects of the factors, followed by analysis of variance (ANOVA) to determine the significance of the factors and the interactions between them.

In vitro release study

In vitro release of the optimized SL-NLC formulation was performed using the dialysis bag technique.[12,13] Before the experiment, the cellulose dialysis tubes (Spectrapore® dialysis tube 2,000–15,000 Mw cutoff) were soaked in the release medium overnight. One milliliter of the selected NLC dispersion was placed in the dialysis bag then tied at both ends. The dialysis tube was immersed in a beaker containing 100 mL of phosphate buffer (pH=7.4) and shaken using a thermostatically controlled shaker (GLF Corp., Burgwedel, Germany) adjusted at 100 strokes per minute maintained at 37°C±0.2°C. At preset time intervals, samples from the release medium were withdrawn and assayed spectrophotometrically. Each withdrawn sample was replaced by an equal volume of fresh release medium. To ascertain the kinetic modeling of drug release, the release data of SL from the selected NLC formulation were fitted to zero order, first order, and Higuchi diffusion models.[14]

Surface morphology by transmission electron microscopy

Morphological parameters including sphericity and aggregation of selected SL-NLC dispersion were examined using transmission electron microscopy (TEM) (JEOL JEM1230, Tokyo, Japan).

Differential scanning calorimetry analysis

Prior to differential scanning calorimetry (DSC) analysis, selected SL-NLC formulation was lyophilized (Novalyphe-NL 500; Savant Instruments Corp., Hicksville, NY, USA) in order to transfer it to dry powders. SL, physical mixture of SL with NLC components, and the lyophilized SL-NLCs were subjected to DSC (PerkinElmer, Waltham, MA, USA) analysis.

X-ray diffraction study

Similar to DSC analysis, selected SL-NLC dispersions were lyophilized. X-ray diffraction (XRD) analysis of SL, physical mixture of SL with NLC components, and lyophilized SL-NLCs of the selected formulation were conducted by powder XRD (Scintag Inc., Santa Clara, CA, USA).

Ex vivo visualization using confocal laser scanning microscopy

Preparation of rhodamine B isocyanate-loaded NLCs

Rhodamine B isocyanate-loaded NLCs (RH-NLCs) were fabricated using the same method employed for preparing SL-NLCs where RH at a concentration of 0.1% (w/w) replaced SL in the selected NLC formulation.

Skin preparation

Newly born albino mice (70±20 g) were sacrificed and their skin was excised, cleaned, and kept in the freezer (−20°C) until needed. Before use, the skin was defrosted and mounted with the stratum corneum facing the donor compartment in Franz diffusion cells. The receptor volume was 10 mL of phosphate-buffered saline at pH 7.4 maintained at 37°C±0.5°C. To simulate the application of the NLCs onto the surface of skin, RH-NLC formulation was spread evenly on the skin surface and remained for 8 hours. Following that, the skin was rinsed with 50% ethanol and then wiped gently before imaging.[15]

Confocal laser scanning microscopy study

The whole skin was sandwiched between a glass slide and a cover slip and examined using inverted confocal laser scanning microscopy (CLSM) (LSM 710, Carl Zeiss, Jena, Germany). The fluorescence of RH was excited at λ_{ex}=485 nm and detected at λ_{em}=595 nm. RH emission was successfully detected at this wavelength, which was far from the background fluorescence caused by either the skin protein

bands or hair follicles.[15] The skin thickness was optically scanned at 1 μm increments from the skin surface (0 μm) to a depth of 24 μm. The skin was then inspected under a 63× objective lens (EC-Plan Neofluar 63×/01.40 Oil DICM27). Images were obtained using optical sectioning z-stack mode, and the mean fluorescence intensity of each image was plotted against skin depth.[15] Further, to observe the distribution of nanocarriers in the skin structure layers, part of the skin sample was sectioned and microscopically examined.

Results and discussion

Selection of SL-NLC ingredients

Compritol® was selected as the solid lipid for the proposed SL-NLCs due to its favorable characteristics exemplified by low cytotoxicity and ability to solubilize lipophilic drugs.[16] Regarding the liquid lipid, olive oil was purposely selected, as it is abundantly employed in different cosmeceuticals based on its beneficial effects on skin and hair.[17] Among various surfactants suitable for topical applications, Tween® 80 was selected due to its accepted regulatory status and success in preparing various NLCs.[18,19] Transcutol®, being biocompatible with the skin, was incorporated into the NLCs as a penetration enhancer.[20] The composition of the prepared SL-NLCs is presented in Table 2.

Analysis of the factorial design

Factorial designs are commonly used to analyze the influence of different variables on the properties of a drug delivery system.[21] The predicted R^2 values were in reasonable agreement with the adjusted R^2 in all responses (approximately 0.2 difference between them) (Table 3).[22,23] Adequate precision measured the signal-to-noise ratio to ensure that the model can be used to navigate the design space.[24] A ratio >4 (the desirable value) was observed in all responses. Polynomial equations were generated to establish the relationship between the factors and the responses. A positive sign before a factor in a polynomial equation indicates a synergistic effect, whereas a negative sign represents an antagonistic effect.[25] Table 4 represents the regression results of the measured responses (coded values) for SL-NLCs. The values of the coefficients X_1–X_3 relate to the effects of these variables on the corresponding response. Coefficients with more than one factor term (X_1X_2, X_1X_3, X_2X_3) represent the interaction terms. The significance of each coefficient was determined on the basis of *P*-values as listed in Table 4. The smaller the *P*-value, the more significant the corresponding coefficient.[18] Three-dimensional response surface plots obtained from fitting the data in the polynomial equation are depicted in Figure 1. These types of plots are useful to study the effect of two factors on a response at a time when the third factor was kept at a constant level. To evaluate the statistical significance of the effects and the interactions between X_1X_2, X_2X_3, and X_1X_3 on each of the responses, ANOVA statistical tests were performed for each factor and are presented in Pareto charts in Figure 2.

Effect of variables

Effect of formulation variables on the percentage EE

The percentage of SL entrapped within the NLCs varied from 74.90%±2.69% to 91.20%±4.53% (Table 2). The high EE% achieved could be attributed to the hydrophobicity of Compritol® associated with imperfections within its lattice that offer space to accommodate drugs.[26] It is worth mentioning that such a high drug load may also be related to SL's lipophilic nature (log *P*-value=2.78).[27]

As depicted in Figure 2A, increasing the liquid lipid, surfactant, or Transcutol® concentrations causes an increase in drug entrapped within the NLCs (*P*-value=0.3666, 0.0588,

Table 2 Experimental runs, independent variables, and measured responses of the 2^3 full factorial experimental design. Data represented as mean ± standard deviation (n=3)

Formula	X_1	X_2	X_3	Y_1	Y_2	Y_3	Y_4
	Liquid lipid[a] (%)	Surfactant[b] (%)	Transcutol®[c] (%)	EE (%)	PS (nm)	PI	ZP (mV)
SL-NLC 1	5	1	0	75.04±1.47	333.7±23.1	0.846±0.037	−26.5±1.27
SL-NLC 2	5	1	50	87.36±3.34	215.6±20.4	0.877±0.023	−18.7±0.92
SL-NLC 3	5	2	0	87.83±2.59	769.5±13.4	0.705±0.021	−17.8±1.13
SL-NLC 4	5	2	50	81.33±1.89	731.5±16.3	0.630±0.028	−21.2±0.49
SL-NLC 5	15	1	0	74.90±2.69	739.4±36.3	0.561±0.032	−25.5±0.71
SL-NLC 6	15	1	50	91.20±4.53	834.3±81.0	0.547±0.009	−24.7±0.92
SL-NLC 7	15	2	0	87.31±1.85	599.5±41.9	0.672±0.101	−21.0±1.41
SL-NLC 8	15	2	50	82.95±1.34	614.7±66.8	0.289±0.016	−22.1±0.64

Notes: [a]Liquid lipid percentage in the total lipid; [b]surfactant percentage in the aqueous phase; [c]Transcutol® concentration in liquid lipid (%).
Abbreviations: SL-NLC, spironolactone-loaded nanostructured lipid carrier; EE, entrapment efficiency; PS, particle size; PI, polydispersity index; ZP, zeta potential.

Table 3 Output data of the 2^3 factorial analysis of spironolactone-loaded nanostructured lipid carrier formulations

Responses	R^2	Adjusted R^2	Predicted R^2	Adequate precision	Significant factors
Entrapment efficiency (%)	0.899764	0.832940	0.683206	9.677522	X_3, X_2X_3
Particle size (nm)	0.968482	0.94747	0.900388	17.75331	X_1, X_2, X_1X_2, X_2X_3
Polydispersity index	0.935639	0.892732	0.796588	14.87902	X_1, X_2, X_3, X_1X_3, X_2X_3
Zeta potential (mV)	0.8010	0.6683	0.3710	6.445	X_2, X_2X_3

and 0.0065, respectively). Previous studies have illustrated that incorporation of liquid lipids to solid lipids causes disturbance in solid lipid crystal order, thus allowing more space to accommodate drug molecules.[12] Generally, the surfactant molecules cover the hydrophobic interface of the dispersed NLCs. At a higher surfactant concentration, part of the drug molecules will be incorporated in the surfactant layer at the surface of the nanoparticles, leading to high EE. Das et al[13] and Yang et al[25] elucidated that a sufficient amount of surfactant is necessary for solubilization and stabilization of drug molecules within the lipid matrix and at the surface of the nanoparticles.[13,25] Significant interaction between the two-factor X_2X_3 was detected ($P<0.0001$). In the absence of Transcutol® in the liquid lipid, the increase in surfactant concentration resulted in a greater increase in the EE% than with the presence of 50% Transcutol® in the liquid lipid (Figure 1A). SL has poor aqueous solubility, which is about 2.8 mg/100 mL at 25°C.[28] A high amount of surfactant and Transcutol® probably increased the solubility of SL in the aqueous phase; thus, the drug may suffer partition from the NLCs to the aqueous medium, causing a decrease in EE%.

Effect of formulation variables on PS

The average PS presented in a z-average diameter of SL-NLCs ranged from 215.6±20.4 nm to 834.3±81.0 nm (Table 2). As shown in Table 4 and the Pareto chart (Figure 2B), the liquid lipid and surfactant concentration had a significantly positive effect on the mean PS ($P<0.05$). Increasing the liquid lipid concentration simultaneously increases the NLCs' PS due to the increase in the amount of the drug entrapped in nanoparticles. The positive relationship of the percentage of surfactant on PS might be attributed to the accumulation of excess surfactant molecules on the NLC surface as a result of the hydrophobic interaction of the nonpolar alkyl chains of the surfactant with solid lipid molecules, resulting in larger PS. A similar finding was reported for bicalutamide-loaded NLCs where a concentration-dependent increase in PS with the increase in surfactant concentration was observed and related to the deposition of the surfactant molecules onto the lipid particles.[12]

On the other hand, the presented interactions (X_1X_2) had a significant effect on the PS of SL-NLCs. At a low surfactant concentration, increasing the liquid lipid results in an increase in the PS to a greater extent than at a high surfactant concentration (Figure 1B). Probably at a high surfactant concentration, the oil is preferentially stabilized within the surfactant micelles rather than inside the NLCs.

Effect of formulation variables on PI

The PI of the prepared NLCs ranged from 0.289±0.016 to 0.877±0.023 (Table 2). As is evident in Table 4 and Figure 2C, all of the investigated variables – namely, liquid lipid, surfactant, and Transcutol® concentrations – had a significant contribution to decreasing the PI (P-value<0.0001, 0.0015, and 0.0050, respectively). The addition of oil favored the formulation of homogeneous particles. In the studies conducted by Hu et al[29] and Agrawal et al[18] the PI of the

Table 4 Regression results of the measured responses (coded values) for spironolactone-loaded nanostructured lipid carriers

Coefficient	Y_1: EE%		Y_2: PS		Y_3: PI		Y_4: ZP	
		P-value		*P*-value		*P*-value		*P*-value
Intercept	83.491		604.756		0.641		22.5	
X_1	0.600	0.3666	92.194	<0.0001*	–0.124	<0.0001*	0.97	0.0623
X_2	1.365	0.0588	74.044	0.0002*	–0.067	0.0015*	–1.75	0.0041*
X_3	2.220	0.0065*	–5.756	0.6515	–0.055	0.0050*	–0.75	0.1362
X_1X_2	–0.326	0.6175	–163.894	<0.0001*	0.030	0.0745	0.075	0.8736
X_1X_3	0.765	0.2565	33.281	0.0243*	–0.044	0.0161*	0.73	0.1481
X_2X_3	–4.933	<0.0001*	0.056	0.9965	–0.059	0.0033*	1.2	0.0279*

Note: *Statistically significant ($P<0.05$).
Abbreviations: EE, entrapment efficiency; PS, particle size; PI, polydispersity index; ZP, zeta potential.

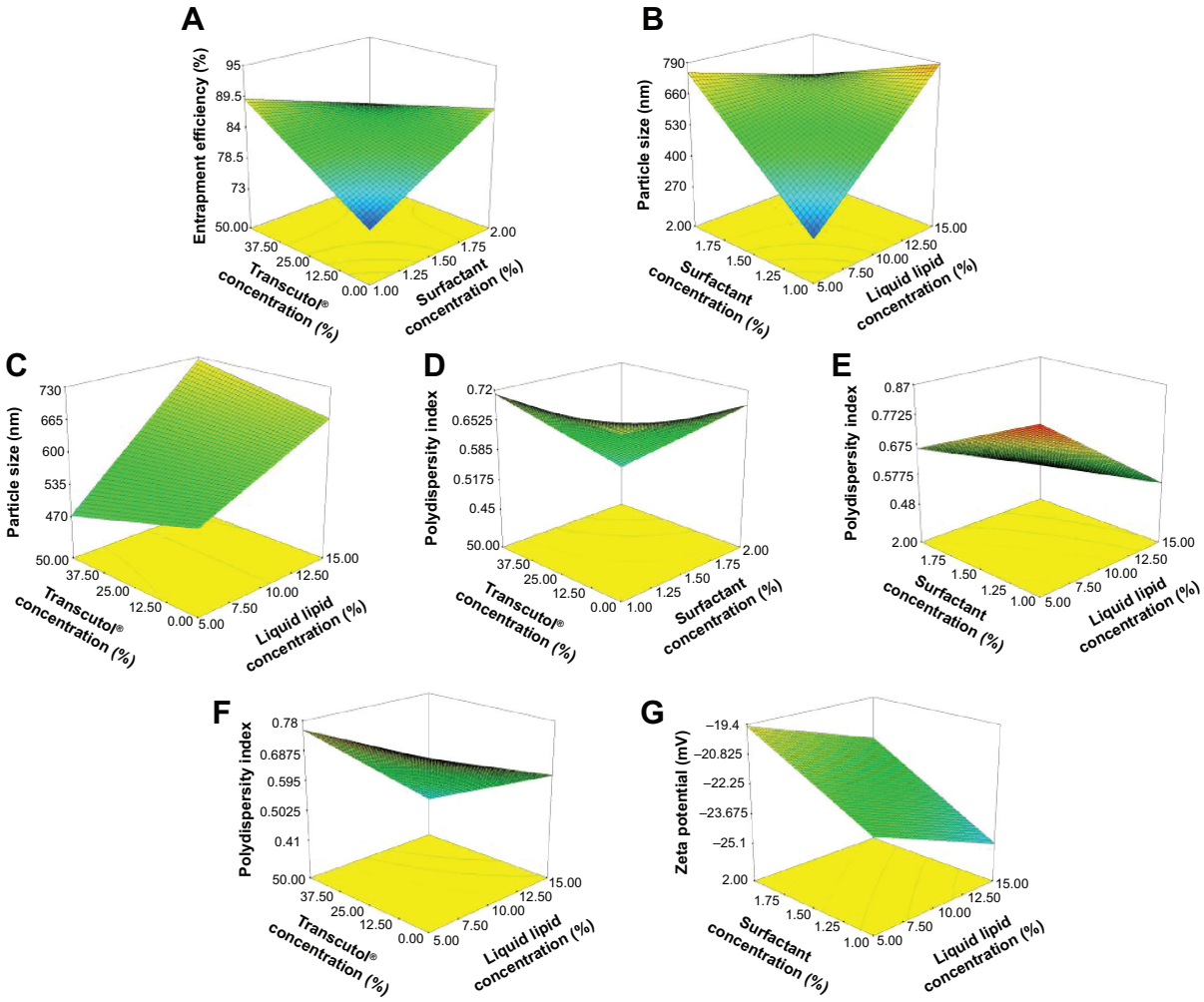

Figure 1 Response surface plots depicting the effect of the variables and the interaction between them on the response.
Notes: (**A**) The effect of the surfactant concentration and Transcutol® concentration on entrapment efficiency, (**B**) the effect of surfactant concentration and liquid lipid concentration on particle size, (**C**) the effect of Transcutol® concentration and liquid lipid concentration on particle size, (**D**) the effect of Transcutol® concentration and surfactant concentration on polydispersity index, (**E**) the effect of surfactant concentration and liquid lipid concentration on polydispersity index, (**F**) the effect of Transcutol® concentration and liquid lipid concentration on particle size, and (**G**) the effect of surfactant concentration and liquid lipid concentration on zeta potential.

NLCs was also decreased by increasing the oleic acid content. Likewise, the increase in surfactant concentration caused a simultaneous decrease in PI. A higher amount of surfactant is required to cover the nanoparticles' surface, stabilizing them and preventing coalescence. Transcutol®, being a cosolvent with low viscosity, reduced the surface tension of the oil droplets, allowing the formation of a homogeneous emulsion during nanoparticle preparation that cooled down to form nanoparticles with the same size range.

The presented interactions (X_1X_3) and (X_2X_3) displayed significant antagonist effects on the response Y_3. This means that a simultaneous increase in the amount of Transcutol® associated with an increase in either the oil or the surfactant concentration leads to a substantial decrease in the PI and favored the forming of more homogeneous distributed nanoparticles (Figure 1D and F).

Effect of formulation variables on ZP

In the present study, the ZP values of the NLCs were in the range of −17.8 to −26.5 mV (Table 2).

The negative charge acquired by the NLCs was related to the ionization of glyceride fatty acids in Compritol® and that of the carboxylic acid groups in olive oil.[30] As is presented in Table 4 and graphically illustrated in Figure 2D, increasing the liquid lipid (X_1) is associated with an increase in ZP, probably due to the increase in the number of ionized carboxylic groups of olive oil present at a higher oil concentration.[31] Conversely, the surfactant concentration has a significant negative effect on ZP as a result of shielding the surface charges of the nanoparticles by the nonionic surfactant molecules. The surfactant molecules decrease the electrostatic repulsion between the nanoparticles, but at the same time sterically stabilize them by forming a surfactant

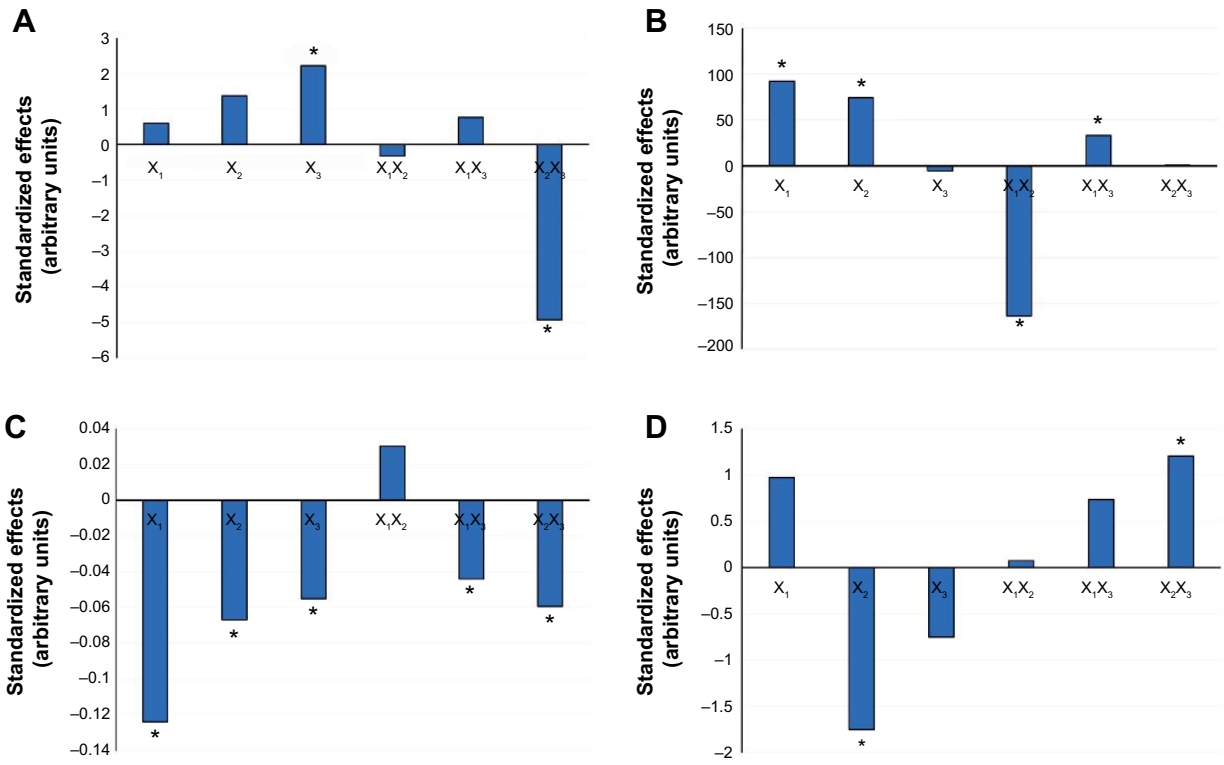

Figure 2 Evaluation of the standardized effects of the percentage liquid lipid with respect to total lipid mixture (X_1), percentage surfactant concentration in aqueous phase (X_2), and percentage of Transcutol® in liquid lipid (X_3) on the (**A**) percentage entrapment efficiency, (**B**) particle size, (**C**) polydispersity index, and (**D**) zeta potential. *Considered statistically significant for *P*-value<0.05.

coat layer. In case of combined electrostatic and steric stabilization, the ZP obtained in our study can be considered sufficient for ensuring the NLCs' physical stability.[12]

Optimization and validation of SL-NLCs

The desirability function combines all the responses into one variable to predict the optimum levels for the studied factors.[32] Accordingly, desirability was calculated to select the optimized formulas with the least PS and PDI along with the highest EE% and ZP (as absolute value). The highest desirability value (0.865) was depicted in the formula SL-NLC 2 (encompassing Compritol® containing 5% liquid lipid [olive oil and Transcutol® 1:1] and emulsified using 1% Tween 80 in the aqueous phase). Hence, this formula was selected for further investigation.

In vitro drug release

The cumulative percentage of SL released from the optimized NLCs (SL-NLC 2) in comparison with drug suspension containing the same drug concentration is depicted in Figure 3.

Under the same experimental conditions, SL suspension (used as a reference) released about 40% of the drug at the end of the 24-hour release study compared with 66% from the optimized formulation. The observed difference in the release pattern between drug suspension and SL-NLCs is possibly related to the solubilizing effect of Tween 80 and Transcutol®, which caused dissolution rate enhancement. Further, it should be noted that the rate of drug dissolution is directly proportional to the surface area of the solute particle. In drug suspension, SL is present in a crystalline form with larger PS (lower surface area) than that in the nanosized formulation. This probably also contributes to lowering the dissolution rate of SL, which is a prerequisite to passing

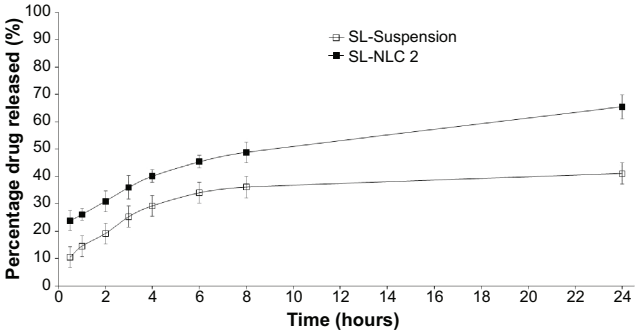

Figure 3 Cumulative percentage of spironolactone released from drug suspension and spironolactone-loaded nanostructured lipid carriers (SL-NLC 2) in phosphate buffer of pH 7.4.
Note: Mean ± standard deviation, n=3.

through the dialysis membrane. This result is consistent with those obtained by Kumbhar and Pokharkar[12] and Elnaggar et al[33] who reported higher drug flux from NLCs than drug suspension across an artificial membrane.

For the NLC formulation, a biphasic drug release pattern characterized by initial burst release followed by a gradual drug release phase was observed. Hu et al[29] reported that when a solvent diffusion method is used for preparing NLCs, the liquid lipid is not homogeneously distributed within the nanoparticles. During the cooling process while preparing the NLCs, because of the difference in the melting point between solid lipid and liquid lipid, the solid lipid (Compritol®), which has a higher melting point, crystallizes first, forming a relatively liquid lipid-free core with most of the liquid lipid at the outer shell of the nanoparticles. The initial burst release might be due to the presence of the liquid lipid on the outer shell of the nanoparticles. Due to the considerably high solubility of lipophilic SL in the liquid lipid, a drug-enriched shell is formed that is considerably soft, from which either the drug can diffuse or the matrix erode.[29,34]

After the initial burst phase, relatively slow drug release was observed, probably due to the penetration of the aqueous diffusion medium into the hydrophobic lipid core followed by slow dissolution followed by drug diffusion. At a later stage, further reduction in drug release occurred due to depletion of the drug from the core lipid matrix, leading to a reduced concentration gradient. The observed release patterns are interesting for follicular application in the view of that the initial release improves the penetration of drug, while further steady release provides the drug over a prolonged period of time.

Based on analyzing the release data of the investigated SL-NLC 2 using different kinetic models, the in vitro release data followed a Higuchi diffusion release model with the best fit r^2 value (r^2=0.979) compared with the other kinetic models (Table 5). This model explains the time-dependent release of drug from an insoluble matrix based on Fickian diffusion.[35] Similar results were reported by Ghasemian et al.[36]

Table 5 Results of model fitting for optimized spironolactone-loaded nanostructured lipid carriers

Models	Slope	r^2	Intercept
Zero order	1.659	0.865	29.505
First order	0.016	0.743	1.475
Higuchi	10.237	0.979	17.768

TEM microscopy

TEM images of the optimized SL-NLC 2 confirmed that the particles were nonaggregated and spherical in shape with narrow size distribution (Figure 4). It was observed from different frames that only single colloidal species were present throughout the investigated sample. The mean size of the particles observed in the TEM micrographs was in good agreement with the size obtained from the PS analyzer (Table 2).

DSC analysis

The diffractograms of pure SL, physical mixture of SL with NLC components, and lyophilized optimum SL-NLCs are shown in Figure 5. The thermogram of SL depicts a characteristic endothermic peak at 206.87°C, which is in agreement with the enthalpy of fusion of SL.[37] Although it is not clearly visualized in the DSC thermogram of the physical mixture of SL with NLC components, the characteristic peak of SL was detected by the DSC apparatus at 207.5°C, confirming that it retained its crystalline nature within the physical mixture.

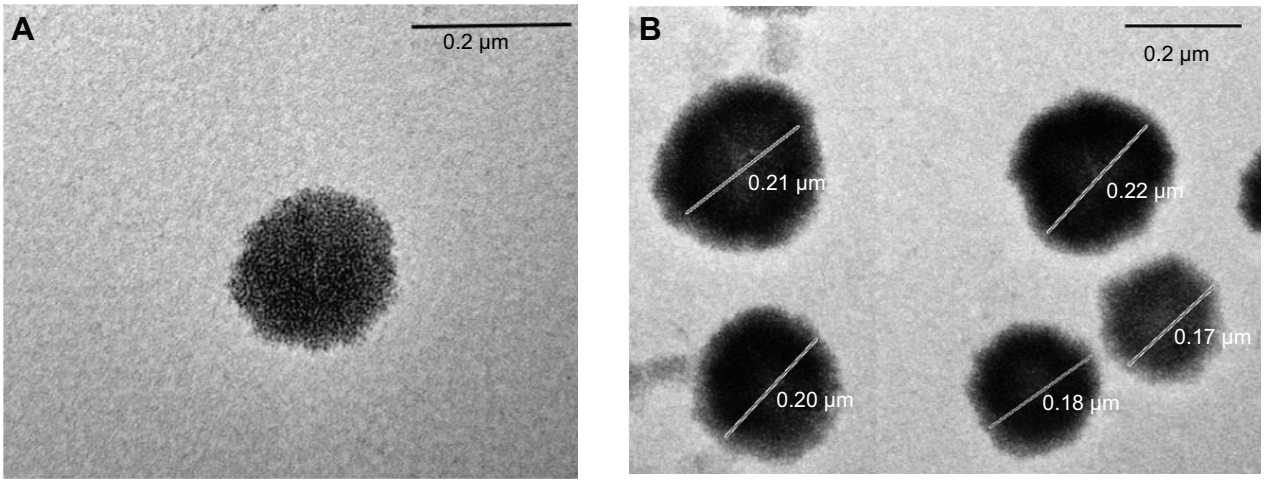

Figure 4 Transmission electron micrographs of the optimized spironolactone-loaded nanostructured lipid carriers displaying (**A**) its spherical structure, and (**B**) non-aggregating orientation.

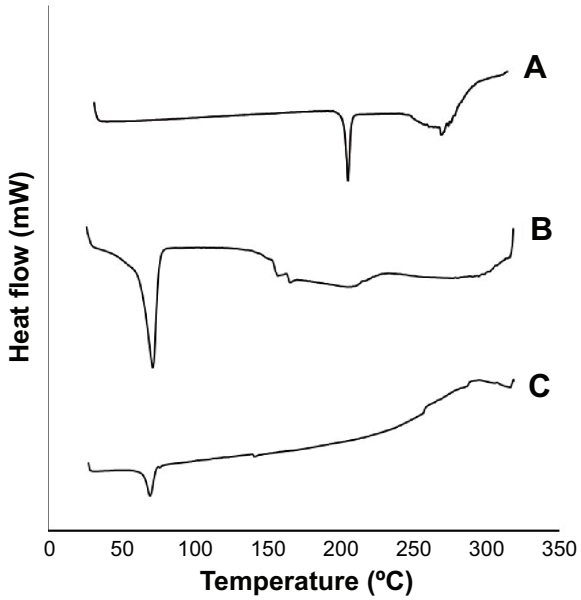

Figure 5 Differential scanning calorimetry thermograms of (**A**) spironolactone, (**B**) physical mixture of spironolactone with nanostructured lipid carrier components, and (**C**) lyophilized spironolactone-loaded nanostructured lipid carriers.

The almost complete masking of SL endothermic peak in the physical mixture could be ascribed to the low concentration of the drug compared with Compritol®, making it hard to detect using DSC.[38] The melting endothermic peak of SL completely disappeared in the lyophilized SL-NLC formulation, indicating that SL was homogeneously dispersed in an amorphous state within the NLCs. It has been reported that the drug endothermic peak wanes in the nanoparticulate formulations due to its presence in an amorphous state.[18] On the other hand, the characteristic endothermic peak of Compritol® (72.07°C) was clearly evident in the physical mixture of the drug with NLC component, confirming Compritol®'s crystalline nature and its presence in β' form.[39,40] There was a decrease in Compritol® peak intensity accompanied by a slight shift of the endothermic peak to the lower temperature side (70.88°C) in the NLC formulation. These changes were attributed to the decrease in PS associated with the increase in surface area of Compritol®, which caused a decrease in melting enthalpy.[41] However, the melting endotherm of Compritol® (70.88°C) signifies that only polymorph β' form was formed during the solidification of the lipid to form the nanoparticles. This result is in agreement with previous studies that provide evidence that Compritol® crystallizes in its β' modification after being exposed to thermal stress.[40,42]

XRD study

X-ray diffractograms of pure SL, a physical mixture of SL with NLC components, and lyophilized optimum SL-NLCs are shown in Figure 6. The diffraction pattern of pure SL exhibited principal high intensity peaks at 9.19, 16.01, 16.67, and 17.29° 2θ, signifying its crystalline nature. In the diffractogram of the physical mixture, the characteristic peaks of Compritol® were present at 21.27° 2θ and at 23.35° 2θ, confirming its crystallinity and presence in β' form, as previously suggested by DSC results.[43] The crystalline peaks of SL at 16.01, 16.67, and 17.29° 2θ were evident but with lower intensities in the physical mixture, confirming the presence of SL in crystalline form. On the contrary, the diffractogram of SL-NLC formulation showed a deformed peak for SL, signifying that the drug lost its crystallinity and was transformed to an amorphous state or molecular dispersion within the nanocarriers. On the other hand, the two characteristic peaks of the β' form of Compritol® were still present in the diffractogram of NLC formulation, confirming that the carrier crystallized into its stable polymorphic form. Nevertheless, the reduction in their intensities specifies that some crystalline modification took place in the final formulation, attributed to disordering of the solid lipid crystalline structure due to the presence of liquid lipid.[44]

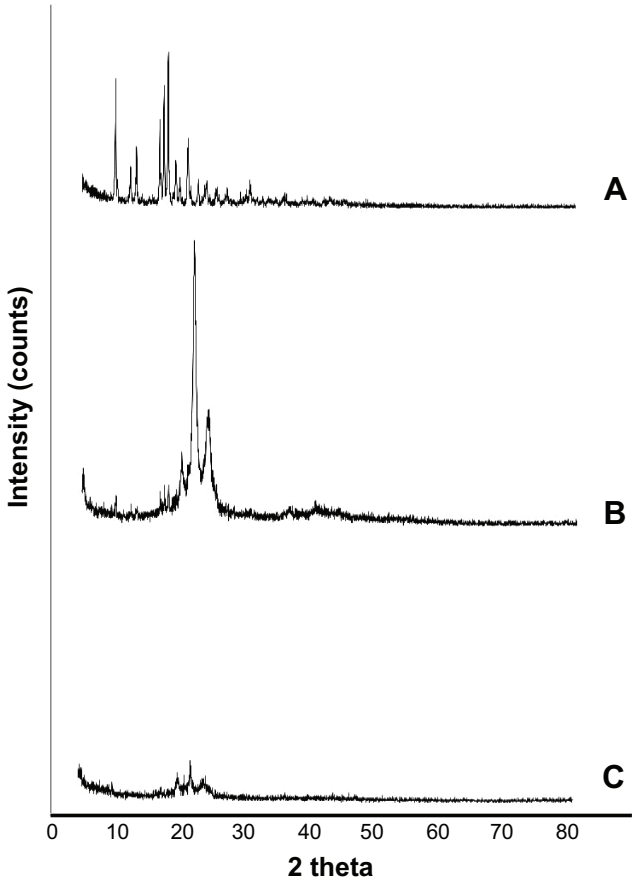

Figure 6 X-ray diffractograms of (**A**) spironolactone, (**B**) physical mixture of spironolactone with nanostructured lipid carrier components, and (**C**) lyophilized spironolactone-loaded nanostructured lipid carriers.

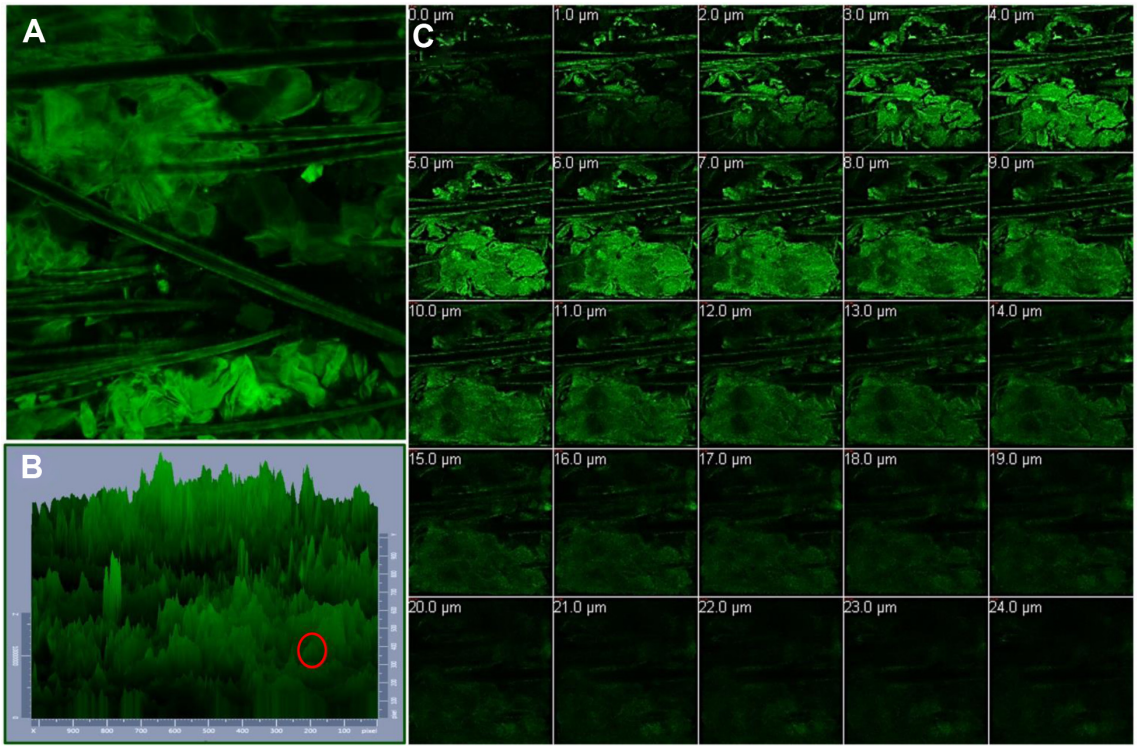

Figure 7 Confocal laser scanning microscopy images.
Notes: Confocal laser scanning microscopy images of (**A**) normal xy image of rat skin treated with nanostructured lipid carriers fluorolabeled with rhodamine B isothiocyanate, (**B**) 1,024×1,024 three-dimensional plot of the same xy image (the hair follicles are localized and circled in red), and (**C**) z-stack image of the stratum corneum sectioned from 0 µm to 24 µm with 1 µm increments.

CLSM

In the current investigation, RH was selected as a model lipid-soluble fluorophore to mimic the behavior of a lipophilic drug in the NLCs.[45] Generally, drug penetration into the skin can occur through the corneocytes (transcellular route), between the corneocytes (intercellular route), and via the appendages.[46]

Figure 7 demonstrates the distribution of the studied RH-NLCs across the skin. Figure 7A presents a normal xy image of rat skin, which is depicted in Figure 7B in the form of a 1,024×1,024 three-dimensional plot. Figure 7C depicts the acquisition of 24 optical sections (x-y plane) taken at successive focal planes along the z axis to obtain three-dimensional information about the penetration of the NLCs within the hair follicles.

As depicted (Figure 7A), there was a widespread distribution of the fluorescence around the hair follicles and hair shafts, probably due to the accumulation of the NLCs within this area, confirming that the hair follicles represent a potential pathway for NLC penetration. It is worth mentioning that within the stratum corneum, the follicular ducts represent intrusions containing lipophilic content due to sebum secretion from the sebaceous gland.[46] In this domain, the lipophilic nature of the proposed NLCs is likely to contribute to follicular penetration. Fluorescence deposition was also present at the outermost layer of the hair structure, probably due to the interaction between the NLCs and hair cuticle.[47]

Though with less intensity than near the hair follicles, the fluorescence of RH was also visible in strata (Figure 8),

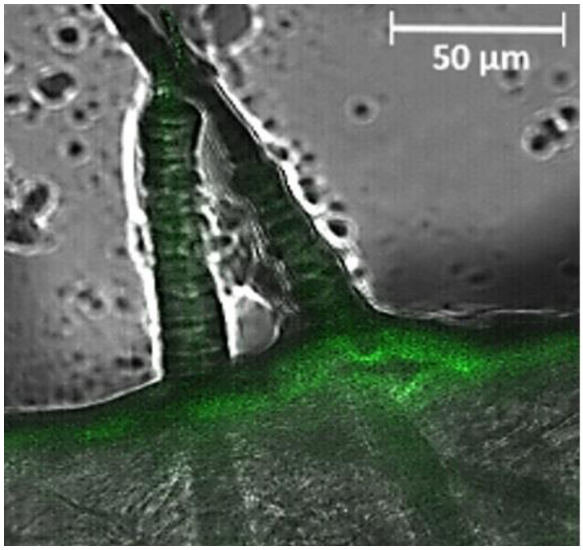

Figure 8 Accumulation of nanostructured lipid carriers fluorolabeled with rhodamine B isothiocyanate within the vicinity of hair follicles.

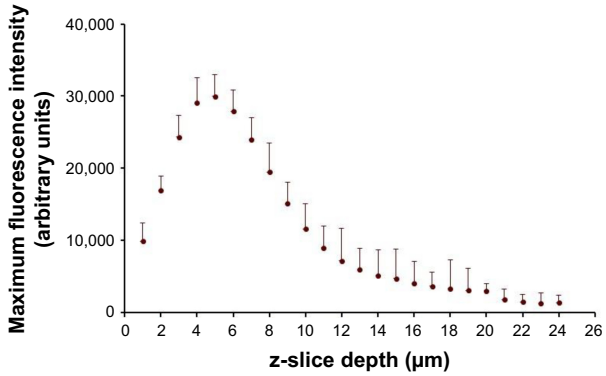

Figure 9 Mean fluorescence intensities of rhodamine B isothiocyanate across the stratum corneum depth.
Note: Mean ± standard deviation, n=3.

which indicates the possibility of the nanoparticles' permeation across the stratum cornea, most likely due to penetration of the NLCs via the intercellular pathway. Previous studies inferred that nanoparticles can closely contact with the furrows between corneocytes and form intercellular deposits that favor accumulation and sustained delivery.[48,49] The proposed NLC system, being lipophilic in nature and containing Transcutol® as a penetration enhancer, may have interacted with the skin surface lipids, facilitating drug penetration through the intercellular route.

Plotting the mean of the fluorescence intensities against the z-slices depth depicted that dye fluorescence was maintained until a depth of 24 μm within the skin (Figure 9).

In summary, CSLM confirmed that the fluorescence intensity of RH-NLCs at the follicular region was relatively higher than at the nonfollicular region, indicating that the follicular pathway was the main penetration pathway of the proposed NLCs. Since the density of hair follicles on the scalp can reach as much as 10% of the total skin surface,[50] it is logically anticipated that the follicular pathway will represent the predominant route of penetration of the proposed NLCs through the scalp.

Conclusion

Optimization of NLCs requires the consideration of different formulation variables and the interactions between them. In this work, NLCs for follicular targeting of SL were successfully prepared using an emulsion solvent diffusion and evaporation method followed by ultrasonication. Using a complete 2^3 factorial design, the derived polynomial equations and response surface plots aided in the preparation of an optimum formulation with the desired properties. The latter was composed of Compritol® containing 5% liquid lipid (olive oil and Transcutol 1:1) and emulsified using 1% Tween 80. This formulation revealed spherical morphology with particle size 215.6±20.4 nm, high drug encapsulation efficiency 87.36%±3.34%, and ZP −18.7±0.92 mV. Biphasic drug release patterns with initial burst release followed by sustained release were displayed by SL-NLCs. DSC and XRD studies confirmed the existence of amorphous SL within the optimized NLC formulation. The ability of the optimized NLC formulation to penetrate and accumulate within the hair follicles was confirmed using CLSM.

Disclosure

The authors report no conflicts of interest in this work.

References

1. Rathnayake D, Sinclair R. Innovative use of spironolactone as an antiandrogen in the treatment of female pattern hair loss. *Dermatol Clin*. 2010;28(3):611–618.
2. Chen WC, Zouboulis CC. Hormones and the pilosebaceous unit. *Dermatoendocrinol*. 2009;1(2):81–86.
3. Levy LL, Emer JJ. Female pattern alopecia: current perspectives. *Int J Womens Health*. 2013;5:541–556.
4. Yazdabadi A, Green J, Sinclair R. Successful treatment of female-pattern hair loss with spironolactone in a 9-year-old girl. *Australas J Dermatol*. 2009;50(2):113–114.
5. Adamopoulos DA, Karamertzanis M, Nicopoulou S, Gregoriou A. Beneficial effect of spironolactone on androgenic alopecia. *Clin Endocrinol (Oxf)*. 1997;47(6):759–760.
6. Burke BM, Cunliffe WJ. Oral spironolactone therapy for female patients with acne, hirsutism or androgenic alopecia. *Br J Dermatol*. 1985;112(1):124–125.
7. Hughes BR, Cunliffe WJ. Tolerance of spironolactone. *Br J Dermatol*. 1988;118(5):687–691.
8. Han F, Li S, Yin R, Liu H, Xu L. Effect of surfactant on the formation and characterization of a new type of colloidal drug delivery system: nanostructured lipid carriers. *Colloids Surf A Physiochem Eng Asp*. 2008;315(1–3):210–216.
9. Knorr F, Lademann J, Patzelt A, Sterry W, Blume-Peytavi U, Vogt A. Follicular transport route-research progress and future perspectives. *Eur J Pharm Biopharm*. 2009;71(2):173–180.
10. Eskandari S, Varshosaz J, Minaiyan M, Tabbakhian, M. Brain delivery of valproic acid via intranasal administration of nanostructured lipid carriers: in vivo pharmacodynamic studies using rat electroshock model. *Int J Nanomedicine*. 2011;6:363–371.
11. Priyanka K, Sathali AA. Preparation and evaluation of montelukast sodium loaded solid lipid nanoparticles. *J Young Pharm*. 2012;4(3):129–137.
12. Kumbhar DD, Pokharkar VB. Engineering of a nanostructured lipid carrier for the poorly water-soluble drug, bicalutamide: physicochemical investigations. *Colloids Surf A Physicochem Eng Asp*. 2013;416:32–42.
13. Das S, Ng WK, Kanaujia P, Kim S, Tan RB. Formulation design, preparation and physicochemical characterizations of solid lipid nanoparticles containing a hydrophobic drug: effects of process variables. *Colloids Surf B Biointerfaces*. 2011;88(1):483–489.
14. Higuchi WI. Analysis of data on the medicament release from ointments. *J Pharm Sci*. 1962;51:802–804.
15. Hathout RM, Nasr M. Transdermal delivery of betahistine hydrochloride using microemulsions: physical characterization, biophysical assessment, confocal imaging and permeation studies. *Colloids Surf B Biointerfaces*. 2013;110:254–260.
16. Manjunath K, Reddy JS, Venkateswarlu V. Solid lipid nanoparticles as drug delivery systems. *Methods Find Exp Clin Pharmacol*. 2005;27(2):127–144.

17. Baumann L, Weisberg E. Olive oil in botanical cosmeceuticals. In: Preedy VR, Watson RR, editors. *Olives and Olive Oil in Health and Disease Prevention*. Oxford, UK: Academic Press; 2010.
18. Agrawal Y, Petkar KC, Sawant KK. Development, evaluation and clinical studies of acitretin loaded nanostructured lipid carriers for topical treatment of psoriasis. *Int J Pharm*. 2010;401(1–2):93–102.
19. Gonzalez-Mira E, Egea MA, Garcia ML, Souto EB. Design and ocular tolerance of flurbiprofen loaded ultrasound-engineered NLC. *Colloids Surf B Biointerfaces*. 2010;81(2):412–421.
20. Mura S, Manconi M, Valenti D, Sinico C, Vila AO, Fadda AM. Transcutol containing vesicles for topical delivery of minoxidil. *J Drug Target*. 2011;19(3):189–196.
21. Araújo J, Gonzalez-Mira E, Egea MA, Garcia ML, Souto EB. Optimization and physicochemical characterization of a triamcinolone acetonide-loaded NLC for ocular antiangiogenic applications. *Int J Pharm*. 2010;393(1–2):167–175.
22. Basalious EB, El-Sebaie W, El-Gazayerly O. Application of pharmaceutical QbD for enhancement of the solubility and dissolution of a class II BCS drug using polymeric surfactants and crystallization inhibitors: development of controlled-release tablets. *AAPS PharmSciTech*. 2011;12(3):799–810.
23. Quinten T, Gonnissen Y, Adriaens E, et al. Development of injection moulded matrix tablets based on mixtures of ethylcellulose and low-substituted hydroxypropylcellulose. *Eur J Pharm Sci*. 2009; 37(3–4):207–216.
24. Lima DL, Calisto V, Esteves VI. Adsorption behavior of 17alpha-ethynylestradiol onto soils followed by fluorescence spectral deconvolution. *Chemosphere*. 2011;84(8):1072–1078.
25. Yang CR, Zhao XL, Hu HY, et al. Preparation, optimization and characteristic of huperzine a loaded nanostructured lipid carriers. *Chem Pharm Bull (Tokyo)*. 2010;58(5):656–661.
26. Jenning V, Thunemann AF, Gohla SH, Characterisation of a novel solid lipid nanoparticle carrier system based on binary mixtures of liquid and solid lipids. *Int J Pharm*. 2000;199(2):67–77.
27. Szasz G, Budvari-Barany Z, editorss. *Pharmaceutical Chemistry of Antihypertensive Agents*. Volume 1. New York, NY: CRC Press; 1990.
28. Overdiek HW, Merkus FW. The metabolism and biopharmaceutics of spironolactone in man. *Rev Drug Metab Drug Interact*. 1987; 5(4):273–302.
29. Hu FQ, Jiang SP, Du YZ, Yuan H, Ye YQ, Zeng S. Preparation and characterization of stearic acid nanostructured lipid carriers by solvent diffusion method in an aqueous system. *Colloids Surf B Biointerfaces*. 2005;45(3–4):167–173.
30. Sanad RA, AbdelMalak NS, ElBayoomy TS, Badawi AA. Formulation of a novel oxybenzone-loaded nanostructured lipid carriers (NLCs). *AAPS PharmSciTech*. 2010;11(4):1684–1694.
31. Huang Z, Hu S, Yang Y, Fang J. Development and evaluation of lipid nanoparticles for camptothecin delivery: a comparison of solid lipid nanoparticles, nanostructured lipid carriers, and lipid emulsion. *Acta Pharmacol Sin*. 2008;29(9):1094–1102.
32. Pandya VM, Patel JK, Patel DJ. Formulation and optimization of nanosuspensions for enhancing simvastatin dissolution using central composite design. *Dissolution Technology*. 2011;18:40–45.
33. Elnaggar YS, El-Massik MA, Abdallah OY. Fabrication, appraisal, and transdermal permeation of sildenafil citrate-loaded nanostructured lipid carriers versus solid lipid nanoparticles. *Int J Nanomedicine*. 2011;6:3195–3205.
34. Jia LJ, Zhang DR, Li ZY, et al. Preparation and characterization of silybin-loaded nanostructured lipid carriers. *Drug Deliv*. 2010; 17(1):11–18.
35. Higuchi T. Mechanism of sustained-action medication. theoretical analysis of rate of release of solid drugs dispersed in solid matrices. *J Pharm Sci*. 1963;52:1145–1149.
36. Ghasemian E, Vatanara A, Rouholamini Najafabadi A, Rouini MR, Gilani K, Darabi M. Preparation, characterization and optimization of sildenafil citrate loaded PLGA nanoparticles by statistical factorial design. *Daru*. 2013;21(1):68.
37. Yassin AE, Alanazi FK, El-Badry M, Alsarra IA, Barakat NS, Alanazi FK. Preparation and characterization of spironolactone-loaded gelucire microparticles using spray-drying technique. *Drug Dev Ind Pharm*. 2009;35(3):297–304.
38. Craig DQ. The mechanisms of drug release from solid dispersions in water-soluble polymers. *Int J Pharm*. 2002;231(2):131–144.
39. Brubach JB, Jannin V, Mahler B, et al. Structural and thermal characterization of glyceryl behenate by X-ray diffraction coupled to differential calorimetry and infrared spectroscopy. *Int J Pharm*. 2007;336(2): 248–256.
40. Souto EB, Mehnert W, Muller RH. Polymorphic behaviour of Compritol888 ATO as bulk lipid and as SLN and NLC. *J Microencapsul*. 2006;23(4):417–433.
41. Bhalekar MR, Pokharkar V, Madgulkar A, Patil N, Patil N. Preparation and evaluation of miconazole nitrate-loaded solid lipid nanoparticles for topical delivery. *AAPS PharmSciTech*. 2009;10(1):289–296.
42. Passerini N, Qi S, Albertini B, Grassi M, Rodriguez L, Craig DQ. Solid lipid microparticles produced by spray congealing: influence of the atomizer on microparticle characteristics and mathematical modeling of the drug release. *J Pharm Sci*. 2010;99(2):916–931.
43. Fini A, Cavallari C, Ospitali F, Gonzalez-Rodriguez ML. Theophylline-loaded compritol microspheres prepared by ultrasound-assisted atomization. *J Pharm Sci*. 2011;100(2):743–757.
44. Gonzalez-Mira E, Nikolić S, Calpena AC, Egea MA, Souto EB, García ML. Improved and safe transcorneal delivery of flurbiprofen by NLC and NLC-based hydrogels. *J Pharm Sci*. 2012;101(2):707–725.
45. Jain A, Mehra NK, Nahar M, Jain NK. Topical delivery of enoxaparin using nanostructured lipid carrier. *J Microencapsul*. 2013;30(7): 709–715.
46. Chourasia R, Jain SK. Drug targeting through pilosebaceous route. *Curr Drug Targets*. 2009;10(10):950–967.
47. Subongkot T, Wonglertnirant N, Songprakhon P, Rojanarata T, Opanasopit P, Ngawhirunpat T. Visualization of ultradeformable liposomes penetration pathways and their skin interaction by confocal laser scanning microscopy. *Int J Pharm*. 2013;441(1–2):151–161.
48. Baroli B, Ennas MG, Loffredo F, Isola M, Pinna R, López-Quintela MA. Penetration of metallic nanoparticles in human full-thickness skin. *J Invest Dermatol*. 2007;127(7):1701–1712.
49. Lv Q1, Yu A, Xi Y, et al. Development and evaluation of penciclovir-loaded solid lipid nanoparticles for topical delivery. *Int J Pharm*. 2009;372(1–2):191–198.
50. Lieb LM, Liimatta AP, Bryan RN, Brown BD, Krueger GG. Description of the intrafollicular delivery of large molecular weight molecules to follicles of human scalp skin in vitro. *J Pharm Sci*. 1997;86(9):1022–1029.